Aerospace Science and Technology 58 (2016) 60–70

Contents lists available at ScienceDirect

Aerospace Science and Technology

www.elsevier.com/locate/aescte

Flexibility influence on passive stability of a spinning solar sail

Xiaosai Hu, Shengping Gong *

School of Aerospace, Tsinghua University, Beijing, 100084, China

ARTICLE INFO

Article history:
Received 24 January 2014
Received in revised form 4 May 2016
Accepted 1 August 2016
Available online 8 August 2016

Keywords:
Spinning solar sail
Flexibility impact
Stability

ABSTRACT

The attitude passive stability design during inclination cranking is developed using a rigid solar sail model. The criterion shows that the solar sail can be stabilized by designing the structure parameters and the spin rate. An oscillation–attitude–orbit dynamical model by hybrid method is employed to quantify the flexibility effect on the passive station keeping. The simulation results indicate that the oscillation has an obvious impact on the attitude and orbit. The oscillation effect is reduced as the spin rate increases, which means a larger spin rate is required to stable the attitude for a flexible solar sail than the rigid one. For some certain spin rates, the passive stability criterion obtained from the rigid model may become invalid. The comparative simulations are implemented to explain this phenomenon by noting the fact that the flexible structural parameter and the solar radiation pressure torque due to sail vibration are different from the rigid one.

1. Introduction

Solar sail is a spacecraft with a large reflective sail membrane propelled by the solar radiation pressure. This propulsion concept has been verified by the successful demonstration missions, such as IKAROS and NanoSail-D. Due to the endless pressure and strong attitude–orbit coupling, the solar sail is considered to enable some new space missions that are difficult for conventional spacecraft, such as the Geostorm Warning Mission [1], GeoSail [2] and asteroid exploration missions [3]. The solar polar sail mission [4] was proposed by NASA for investigating the cycle of the sun. However, the high orbit inclination means consuming too much fuel for regular spacecraft. Solar sail is a feasible option to achieve a high-inclination heliocentric orbit by inclination cranking. As the propulsion varies in proportion to the inverse square solar distance, the solar sail is usually transferred to a small circle radius for inclination cranking, then the other orbital elements are adjusted to the object value [5]. Due to the characteristic acceleration of solar sail, the attitude should be kept fixed on half of the orbit and a slew maneuver be implemented over each orbit during inclination cranking [6].

Abundant of works discussed the attitude control of solar sail, where the control strategy can be classified as the active control and passive control. The passive control of solar sail, which means no extra control forces except for the solar radiation pressure, was first investigated by McInnes [7]. Most previous literatures focused on the rigid solar sail model, but the oscillation of the sail is rarely studied in the passive design. Gong [8,9] discussed the passive attitude control of three-axis stabilized solar sail relying on the specific shape of the rigid sail. The successful IKAROS mission reignited people's interests to study the spinning solar sail. Mimasu et al. [10] used the solar radiation pressure to control the orientation of a spinning solar sail via adjusting its spin rate. Gong [11] investigated the spin-stabilized design using a rigid model for displaced solar orbit. In fact, for the spinning solar sail with a large flexible membrane deployed by the central force, the flexibility of the sail may have adverse impact to the attitude control, which has become one of the major challenges for attitude control design.

Many flexible models for attitude control were proposed in the previous literatures. Smith [12] distributed the sail mass into the support booms, and the vibration of the booms is analyzed by the mode superposition method. Nakano [13] investigated the stability of a spinning solar sail containing a huge flexible membrane using a free-oscillation analytical model. To be finer, the finite element model developed by the nonlinear FE model can be used to simulate the deformation of the gossamer sail [14–16]. However, the efficiency of the software is usually too low to meet the real-time control require. Likins [17,18] proposed the hybrid coordinate concept to study the coupling effect of the structure oscillation. The elastic deformation of flexible part is described in the floating frame, which can be simplified by modal reduction. Taleghani et al. developed two square sail models using both the MSC/NASTRAN and ABAQUS finite element programs, including geometrically non-

* Corresponding author.
E-mail addresses: huxs12@126.com (X. Hu), gongsp@mail.tsinghua.edu.cn (S. Gong).

http://dx.doi.org/10.1016/j.ast.2016.08.005
1270-9638/

Nomenclature

μ	Gravitational constant of the sun ..... $\mathrm{N\,m^2/kg}$
AU	Average distance between sun and earth ..... 1 AU $= 1.496 \times 10^{11}$ m
m	Mass of the solar sail ..... kg
ρ	The density of the sail membrane ..... $\mathrm{kg/m^3}$
h	The thickness of the sail membrane ..... m
I_t	Rotational inertia along the x_c or y_c axis of the mass center reference frame ..... $\mathrm{kg\,m^2}$
I_s	Rotational inertia along spin axis ..... $\mathrm{kg\,m^2}$
I_{st}	The ratio of I_s and I_t
A	Area of the sail membrane ..... $\mathrm{m^2}$
$\boldsymbol{p}_{\mathrm{sun}}$	The solar radiation pressure exerted on the sail membrane ..... Pa
$p_s/p_{n1}/p_{n2}$	The SRP coefficients of the sail membrane
$C_{spe}/C_{dif}/C_{abs}$	The specular/diffusion/absorption coefficients of the sail membrane 0.72/0.12/0.16
B_f	Lambertian coefficient of the sail front 0.79
κ	thermal emissivity of the sail front 0.05
S_0	the solar constant ..... $1357\ \mathrm{W/m^2}$
$\boldsymbol{c}$	the speed of light ..... 2.998×10^8 m/s
$\boldsymbol{n}$	Unit vector along the sail normal
$\boldsymbol{s}$	Unit vector along the sun-sail line
$\boldsymbol{r}$	Position vector of the sail with respect to the sun
ϕ, α, ψ	Euler angles from the orbital frame to the rotation-free frame ..... rad
$\boldsymbol{\Lambda}$	$[\phi, \alpha, \psi]^{\mathrm{T}}$
$\omega_x, \omega_y, \omega_z$	Angular velocity describing the rotation velocity from the orbital frame to rotation-free frame ... rad/s
Ω_{s}	Spin angle velocity of solar sail ..... rad/s
Ω_{sI}	The product of Ω_{s} and I_{st} ..... rad/s
ω_{o}	Orbital angular velocity of solar sail ..... rad/s
t	Time ..... s
SRP	Abbreviation, solar radiation pressure
cm	Abbreviation, center mass of the solar sail
cp	Abbreviation, center of solar radiation pressure
d	The offset between cm and cp ..... m
IRF	Abbreviation, Inertial Reference Frame
ORF	Abbreviation, Orbital Reference Frame
RFRF	Abbreviation, Rotation-Free Reference Frame
BRF	Abbreviation, Body Reference Frame
MCRF	Abbreviation, Mass Center Reference Frame
λ	Eigenvalue of the coefficient matrix of the linearized system
$\boldsymbol{R}_{\mathrm{O}}$	The global position vector of the origin O
$\boldsymbol{r}_{\mathrm{f}}$	The local position vector in the undeformed state
$\boldsymbol{u}_{\mathrm{f}}$	The local transversal displacement vector of any point in the membrane
x, y	The x and y coordinates of any sail point in the BRF
x_0, y_0	A reference point on the middle surface with zero longitudinal displacement
z	The z coordinate of the point in the membrane
$w(x, y, t)$	The transversal deflection on the middle surface . m
$\boldsymbol{\Phi}$	The mode shape matrix obtained via the finite element model
$\boldsymbol{q}$	The modal coordinate matrix
n	The number of modes applied for modal reduction ..... $n = 3$
δ	The symbol of variation process
$\boldsymbol{I}_3$	The 3×3 unit matrix
$\boldsymbol{S}_0, \boldsymbol{S}_{\mathrm{f}}$	The static moment matrix of the rigid or flexible solar sail
$\boldsymbol{J}_0, \boldsymbol{J}_{\mathrm{f}}$	The rotational inertia matrix of the rigid or flexible solar sail
$\boldsymbol{F}_{\mathrm{t}}, \boldsymbol{F}_{\mathrm{r}}, \boldsymbol{F}_{\mathrm{f}}$	The SRP propulsion, rotation torque, restoring force vector
$\boldsymbol{F}_{\mathrm{gt}}, \boldsymbol{F}_{\mathrm{gr}}, \boldsymbol{F}_{\mathrm{gf}}$	The propulsion, rotation torque, restoring force vector conducted by the gravitation
n_tot	The total number of nodes in sail FE model
e_tot	The total number of shell elements in sail FE model
$(\dot{})(\ddot{})$	The first time and second derivative with respect to the IRF
$(')('')$	The first time and second derivative with respect to the BRF
$(\tilde{})$	The cross product matrix of the vector

linear effects in the structural dynamics analysis [19]. Based on this work, Li et al. [20] developed a reduced dynamical model of a flexible sail with a hybrid coordinate method in the reference floating frame. The satisfactory accuracy and efficiency were verified using the nonlinear FE software ABAQUS/Explicit. The coupling of sail oscillation and attitude–orbit dynamics were considered in the reduced dynamical model.

The passive stability design of a flexible solar sail is studied in this paper. First, the attitude passive keeping strategy for a spinning rigid solar sail in inclination cranking is developed, while the attitude slew maneuver is not discussed. Then, a reduced oscillation–attitude–orbit model is employed to quantify the oscillation influence of the flexible sail on the attitude keeping and the orbit. The mechanism of the oscillation influence is investigated through comparative simulations.

2. Attitude passive stability design using rigid model

The rigid model means that the spin sail is employed into a no deformable plane under the centrifugal force. The attitude dynamics uncoupled with orbit dynamics is served as the station stability design model in this section. Firstly, the five referred rectangular frames are presented, which are applicable to full text. Then the dynamics of solar sail is introduced. Based on the rigid model, the designed attitude equilibrium position and the analytical criterion of attitude passive stability are developed.

2.1. Reference frame definition and transition

For describing the orbit and attitude dynamics of solar sail, five right-hand rectangular frames are defined: the inertial reference frame $OXYZ$, the orbital reference frame $ox_{\mathrm{o}}y_{\mathrm{o}}z_{\mathrm{o}}$, the body reference frame $ox_{\mathrm{b}}y_{\mathrm{b}}z_{\mathrm{b}}$, the mass center reference frame $ox_{\mathrm{c}}y_{\mathrm{c}}z_{\mathrm{c}}$, the rotation-free reference frame $ox_{\mathrm{rf}}y_{\mathrm{rf}}z_{\mathrm{rf}}$. The details of the reference frames are shown in Table 1.

The ORF (Orbital Reference Frame) can be determined by the orbital position and velocity vector in IRF (Inertial Reference Frame).

$$\boldsymbol{A}_{\mathrm{io}} = \begin{bmatrix} \dfrac{(\boldsymbol{r} \times \dot{\boldsymbol{r}}) \times \boldsymbol{r}}{|(\boldsymbol{r} \times \dot{\boldsymbol{r}}) \times \boldsymbol{r}|} & \dfrac{\boldsymbol{r} \times \dot{\boldsymbol{r}}}{|\boldsymbol{r} \times \dot{\boldsymbol{r}}|} & \dfrac{\boldsymbol{r}}{r} \end{bmatrix} \tag{1}$$

The RFRF (Rotation-Free Reference Frame) is obtained by three Euler angles (ϕ, α, ψ) of a rotational sequence of $R_3(\psi) \leftarrow R_1(\alpha) \leftarrow R_3(\phi)$ from the ORF.

$$\boldsymbol{A}_{\mathrm{rfo}} = R_3(\psi) \cdot R_1(\alpha) \cdot R_3(\phi) \tag{2}$$

where $R(\cdot)$ is the standard transition matrix defined in reference literature [21] (listed below):

Table 1
Definition of reference frames.

Name of reference frames	Origin	Frame axes
Inertial reference frame	Mass center of sun	OZ axis is perpendicular to the ecliptic plane, OX axis is in the ecliptic plane and points to the equinox
Orbital reference frame	Geometric center of sail membrane	oz_o axis is along the line from sun to sail, oy_o axis points to direction of the solar sail momentum around the sun
Body reference frame	Geometric center of sail membrane	ox_b and oy_b axes lie in the plane of sail membrane and coincide with the principal axis of inertia. The frame is also defined as the floating frame
Mass center reference frame	Mass center of the whole solar sail	the three axes are parallel to the body reference frame
Rotation-free reference frame	Geometric center of sail membrane	oz_{rf} axis aligns with the body frame oz_b axis, whereas ox_{rf} and oy_{rf} axes do not rotate with the spin of the body

$$R_1(\theta)=\begin{bmatrix}1 & 0 & 0\\ 0 & \cos\theta & \sin\theta\\ 0 & -\sin\theta & \cos\theta\end{bmatrix}$$
$$R_2(\theta)=\begin{bmatrix}\cos\theta & 0 & -\sin\theta\\ 0 & 1 & 0\\ \sin\theta & 0 & \cos\theta\end{bmatrix}$$
$$R_3(\theta)=\begin{bmatrix}\cos\theta & \sin\theta & 0\\ -\sin\theta & \cos\theta & 0\\ 0 & 0 & 1\end{bmatrix}$$

The angular velocity of the RFRF respect to ORF can be described as

$$\boldsymbol{\omega}_{313}\begin{bmatrix}\omega_x\\ \omega_y\\ \omega_z\end{bmatrix}=\begin{bmatrix}\sin\alpha\cdot\sin\psi & \cos\psi & 0\\ \sin\alpha\cdot\cos\psi & -\sin\psi & 0\\ \cos\alpha & 0 & 1\end{bmatrix}\cdot\begin{bmatrix}\dot\phi\\ \dot\alpha\\ \dot\psi\end{bmatrix}=\boldsymbol{A}_\Lambda\cdot\dot{\boldsymbol{\Lambda}} \tag{3}$$

where the matrix of Euler angles

$$\boldsymbol{\Lambda}=[\phi\quad\alpha\quad\psi]^{\mathrm{T}} \tag{4}$$

Eq. (3) also indicates the differential equation of attitude Euler angles

$$\begin{bmatrix}\dot\phi\\ \dot\alpha\\ \dot\psi\end{bmatrix}=\begin{bmatrix}\frac{\sin\psi}{\sin\alpha} & \frac{\cos\psi}{\sin\alpha} & 0\\ \cos\psi & -\sin\psi & 0\\ -\cot\alpha\sin\psi & -\cot\alpha\cos\psi & 1\end{bmatrix}\cdot\begin{bmatrix}\omega_x\\ \omega_y\\ \omega_z\end{bmatrix}=\boldsymbol{A}_\omega\cdot\boldsymbol{\omega}_{313} \tag{5}$$

The BRF (Body Reference Frame) can be attained by spin rotation of RFRF

$$\boldsymbol{A}_{\mathrm{brf}}=R_3(\Omega_s\cdot t)=\begin{bmatrix}\cos(\Omega_s t) & \sin(\Omega_s t) & 0\\ -\sin(\Omega_s t) & \cos(\Omega_s t) & 0\\ 0 & 0 & 1\end{bmatrix} \tag{6}$$

where Ω_s is the spin angle velocity of solar sail.

2.2. Orbit and attitude dynamics of the rigid model

A two-body dynamics model is employed during the inclination cranking. The perturbation extra force exerted on the solar sail are limited to solar radiation pressure propulsion and solar radiation pressure torque.

The orbital dynamical equation in the IRF can be described as

$$\ddot{\boldsymbol{r}}=-\frac{\mu}{r^3}\boldsymbol{r}+\frac{\boldsymbol{F}_t}{m} \tag{7}$$

The attitude dynamical equation in the BRF can be given by

$$\boldsymbol{J}_c\dot{\boldsymbol{\omega}}_b+\boldsymbol{\omega}_b\times\boldsymbol{J}_c\boldsymbol{\omega}_b=\boldsymbol{T}_b \tag{8}$$

Eq. (8) is derived in MCRF (Mass Center Reference Frame). Noting that BRF is parallel to MCRF, the matrix form of the components in Eq. (8) can be written as

$$\boldsymbol{J}_c=\begin{bmatrix}I_t & & \\ & I_t & \\ & & I_s\end{bmatrix},\qquad \boldsymbol{\omega}_b=\begin{bmatrix}\omega_x^b\\ \omega_y^b\\ \omega_z^b\end{bmatrix},\qquad \boldsymbol{T}_b=\begin{bmatrix}T_x^b\\ T_y^b\\ T_z^b\end{bmatrix}, \tag{9}$$

A general SRP (Solar Radiation Pressure) model [22,23] is applied and the force $\mathrm{d}\boldsymbol{F}$ exerted on a small surface $\mathrm{d}A$ is expressed by

$$\begin{aligned}&\mathrm{d}\boldsymbol{F}=\boldsymbol{p}_{\mathrm{sun}}\cdot\mathrm{d}A\\ &\boldsymbol{p}_{\mathrm{sun}}=p_s\cdot(\boldsymbol{s}\cdot\boldsymbol{n})\cdot\boldsymbol{s}+p_{n1}\cdot(\boldsymbol{s}\cdot\boldsymbol{n})^2\cdot\boldsymbol{n}+p_{n2}\cdot(\boldsymbol{s}\cdot\boldsymbol{n})\cdot\boldsymbol{n}\end{aligned} \tag{10}$$

The SRP coefficients in Eq. (10) are obtained by

$$\begin{aligned}p_{n1}&=\frac{S_0}{c}\left(\frac{1}{\mathrm{AU}}\right)^2(2C_{\mathrm{spe}}),\\ p_{n2}&=\frac{S_0}{c}\left(\frac{1}{\mathrm{AU}}\right)^2(B_f C_{\mathrm{dif}}+\kappa C_{\mathrm{abs}}),\\ p_s&=\frac{S_0}{c}\left(\frac{1}{\mathrm{AU}}\right)^2(C_{\mathrm{abs}}+C_{\mathrm{dif}}),\end{aligned} \tag{11}$$

where C_{spe}, C_{dif} and C_{abs} are the specular, diffusion, and absorption coefficients of the sail membrane, respectively; B_f and κ are the Lambertian coefficient and thermal emissivity of the sail front, respectively; S_0, c and AU are the solar constant, the speed of light and the distance to the sun in astronomical units, respectively. The values of these parameters are listed in the nomenclatures.

The matrixes of vector $\boldsymbol{s}$ and $\boldsymbol{n}$ in the BRF are

$$\boldsymbol{s}_b=\boldsymbol{A}_{\mathrm{brf}}\cdot\boldsymbol{A}_{\mathrm{rfo}}\cdot\boldsymbol{s}_o=\boldsymbol{A}_{\mathrm{bo}}\cdot\begin{bmatrix}0\\ 0\\ 1\end{bmatrix},\qquad \boldsymbol{n}_b=\begin{bmatrix}0\\ 0\\ 1\end{bmatrix} \tag{12}$$

Substitute Eq. (12) into Eq. (10) and integrate at the whole sail membrane. The total SRP propulsion and torque with respect to mass center in the BRF can be given by

$$\boldsymbol{F}_b=\begin{bmatrix}p_sA\cdot\cos\alpha\cdot(\cos\Omega_s t\cdot\sin\psi\sin\alpha+\sin\Omega_s t\cdot\cos\psi\cdot\sin\alpha)\\ p_sA\cdot\cos\alpha\cdot(-\sin\Omega_s t\cdot\sin\psi\sin\alpha+\cos\Omega_s t\cdot\cos\psi\cdot\sin\alpha)\\ p_s\cdot\cos^2\alpha+p_{n1}\cdot\cos^2\alpha+p_{n2}\cdot\cos\alpha\end{bmatrix} \tag{13}$$

$$\begin{aligned}\boldsymbol{T}_b&=\boldsymbol{T}_o-\boldsymbol{\rho}_C^b\times\boldsymbol{F}_b\\ &=\begin{bmatrix}p_sA\cdot\cos\alpha\cdot d\cdot(-\sin\Omega_s t\cdot\sin\psi\sin\alpha+\cos\Omega_s t\cdot\cos\psi\cdot\sin\alpha)\\ -p_sA\cdot\cos\alpha\cdot d\cdot(\cos\Omega_s t\cdot\sin\psi\sin\alpha+\sin\Omega_s t\cdot\cos\psi\cdot\sin\alpha)\\ 0\end{bmatrix}\end{aligned} \tag{14}$$

where $\boldsymbol{\rho}_C^b$ is the position matrix of mass center in the BRF and it is assumed as the following form

$$\boldsymbol{\rho}_C^b=\begin{bmatrix}0\\ 0\\ d\end{bmatrix} \tag{15}$$

$\boldsymbol{T}_o$ is the total SRP torque with respect to origin of the BRF

$$\boldsymbol{T}_{\mathrm{o}} = \begin{bmatrix} 0 \\ 0 \\ 0 \end{bmatrix} \tag{16}$$

The matrix of solar sail's angular velocity in the BRF can be described as

$$\boldsymbol{\omega}_{\mathrm{b}} \boldsymbol{A}_{\mathrm{brf}} \cdot \left(\boldsymbol{A}_{\mathrm{rfo}} \cdot \begin{bmatrix} 0 \\ \omega_{\mathrm{o}} \\ 0 \end{bmatrix} + \begin{bmatrix} \omega_x \\ \omega_y \\ \omega_z \end{bmatrix} + \begin{bmatrix} 0 \\ 0 \\ \Omega_{\mathrm{s}} \end{bmatrix} \right) \tag{17}$$

Then the projection of attitude equation in the BRF can be obtained by substituting Eqs. (9), (13), (14) and (17) into Eq. (8). During the inclination cranking, the angular velocity ω_x, ω_y and ω_{o} are small. If it is assumed that the nonlinear items about ω_x, ω_y and ω_{o} can be eliminated, the attitude dynamical equation in the BRF can be simplified into the form

$$\begin{bmatrix} I_t \cdot \dot{\omega}_x \\ I_t \cdot \dot{\omega}_y \end{bmatrix} = \begin{bmatrix} -p_s A \cdot \sin\alpha \cdot \cos\alpha \cdot \sin\psi \cdot d \\ \quad + I_s \Omega_{\mathrm{s}} (\omega_{\mathrm{o}} \cos\psi \cdot \sin\phi + \omega_{\mathrm{o}} \sin\psi \cdot \cos\phi \cdot \cos\alpha + \omega_x) \\ p_s A \cdot \sin\alpha \cdot \cos\alpha \cdot \cos\psi \cdot d \\ \quad + I_s \Omega_{\mathrm{s}} (\omega_{\mathrm{o}} \sin\psi \cdot \sin\phi - \omega_{\mathrm{o}} \cos\psi \cdot \cos\phi \cdot \cos\alpha - \omega_y) \end{bmatrix} \tag{18}$$

It is noted that the z-component in attitude equation is decoupled from the other two. For the spin solar sail the x and y components of the attitude dynamics are preferred, as shown in Eq. (18). This equation is used to design the stable attitude equilibrium position in the paper, and it is called in this paper the design model of passive station keeping.

2.3. Design criterion for passive station keeping

In the inclination cranking, the orientation of solar sail only requires to be changed twice over each orbital loop. In other words, the Euler angle ϕ in this paper needs to be changed between 0 and π rad. During the half orbital loop, the attitude orientation is kept fixed. The required constant attitude Euler angles $\boldsymbol{\Lambda}_0$ ($\alpha = \alpha_0$, $\psi = \psi_0$, $\phi = 0$ or π) over half loop can be designed as the attitude equilibrium point. The condition for the equilibrium is

$$\dot{\omega}_x = 0, \qquad \dot{\omega}_y = 0, \qquad \omega_x = 0, \qquad \omega_y = 0 \tag{19}$$

United with the design model Eq. (18), the condition when the attitude position is an equilibrium point becomes

$$d = \begin{cases} \frac{I_s \Omega_{\mathrm{s}} \cdot \omega_{\mathrm{o}}}{p_s A \cdot \sin\alpha_0} & (\phi = 0) \\ -\frac{I_s \Omega_{\mathrm{s}} \cdot \omega_{\mathrm{o}}}{p_s A \cdot \sin\alpha_0} & (\phi = \pi) \end{cases} \tag{20}$$

The condition indicates that attitude equilibrium position is relevant to the structural parameters I_s and A, pressure parameter p_s, the cm/cp (Abbreviation, cm: center mass of the solar sail; cp: center of solar radiation pressure) offset d and spin velocity Ω_{s}. The required attitude position can be obtained by changing the offset or spin velocity, except for altering the solar sail's inherent parameters. The large maneuver of Euler angle ϕ over one loop can be achieved by two means: reverse the spin velocity or the cm/cp offset. The method of adjusting the offset is employed in this paper as the payload only need to move along the spin axis, while reversing the spin orientation is difficult for the large membrane. If the attitude equilibrium position is given, the required cm/cp offset can be determined by the left parameters in Eq. (20). To be specific, the larger the sail area is, the required cm/cp offset is larger as the ratio of rotational inertia and area size becomes bigger. A large spin rate also needs a large offset to obtain the equilibrium point. On the other hand, if different orbits for inclination cranking are considered the further from the sun the larger offset is required for the balance.

Only the stable attitude equilibrium can guarantee the station keeping in a passive way. A linear stability method is adopted to analyze the stability of the equilibrium point. The method requires the linearized equation from the original system. It is achieved by linearizing the perturbation equation around the equilibrium position. The stability result is obtained by analyzing the linearized system rather than the complicated original system. It should be noted that the linear analysis only provides necessary conditions for stability and sufficient conditions for instability.

The original attitude equation (18) and (5) can be rewritten as

$$\begin{aligned} &\dot{\boldsymbol{X}} = \boldsymbol{f}(\boldsymbol{X}) \\ &\boldsymbol{X} = \begin{bmatrix} \omega_x & \omega_y & \boldsymbol{\Lambda}^{\mathrm{T}} \end{bmatrix}^{\mathrm{T}} \end{aligned} \tag{21}$$

The attitude equilibrium point can be rewritten as

$$\boldsymbol{X}_0 = \begin{bmatrix} 0 & 0 & \boldsymbol{\Lambda}_0^{\mathrm{T}} \end{bmatrix}^{\mathrm{T}} \tag{22}$$

The linearized perturbation equation around $\boldsymbol{X}_0$ is

$$\delta \dot{\boldsymbol{X}} = \boldsymbol{A}_\delta \cdot \delta \boldsymbol{X} \tag{23}$$

where the coefficient matrix of the linearized system

$$\boldsymbol{A}_\delta = \left[\frac{\delta \boldsymbol{f}}{\delta \omega_x} \quad \frac{\delta \boldsymbol{f}}{\delta \omega_y} \quad \frac{\delta \boldsymbol{f}}{\delta \boldsymbol{\Lambda}} \right] \Big|_{\boldsymbol{X} = \boldsymbol{X}_0} \tag{24}$$

The stability of the equilibrium point requires that the real part of eigenvalues of $\boldsymbol{A}_\delta$ is not positive. The characteristic polynomial of $\boldsymbol{A}_\delta$ is

$$\begin{aligned} &\lambda \cdot \left[\lambda^4 - (a_{32} \cdot a_{23} + a_{52} \cdot a_{25} + a_{21} \cdot a_{12} + a_{14}) \lambda^2 \right. \\ &\quad \left. + a_{32} \cdot a_{23} \cdot a_{14} + a_{52} \cdot a_{14} \cdot a_{25} \right] = 0 \end{aligned} \tag{25}$$

where the constant coefficients are

$$\begin{aligned} &a_{12} = -\Omega_{\mathrm{sl}}, \qquad a_{21} = \Omega_{\mathrm{sl}}, \qquad a_{32} = \frac{1}{\sin\alpha_0}, \qquad a_{23} = \Omega_{\mathrm{sl}} \omega_{\mathrm{o}} \\ &a_{25} = 0, \qquad a_{52} = \frac{-\cos\alpha_0}{\sin\alpha_0}, \qquad a_{14} = \frac{\Omega_{\mathrm{sl}} \omega_o \cos^2\alpha_0}{\sin\alpha_0} \end{aligned} \tag{26}$$

Base on the stability polynomial theory, it is possible to make the system marginally stable, whereas it cannot be asymptotic stable [24]. The following criteria must be satisfied for marginal stability

$$\begin{cases} \Omega_{\mathrm{sl}}^2 - \dfrac{\Omega_{\mathrm{sl}} \cdot \omega_{\mathrm{o}}}{\sin\alpha_0} - \dfrac{\Omega_{\mathrm{sl}} \cdot \omega_{\mathrm{o}} \cdot \sin^2\alpha_0}{\sin\alpha_0} \geq 0 \\ \left(\Omega_{\mathrm{sl}}^2 - \dfrac{\Omega_{\mathrm{sl}} \cdot \omega_{\mathrm{o}}}{\sin\alpha_0} - \dfrac{\Omega_{\mathrm{sl}} \cdot \omega_{\mathrm{o}} \cdot \sin^2\alpha_0}{\sin\alpha_0} \right)^2 - \dfrac{4 \cdot \Omega_{\mathrm{sl}}^2 \omega_0^2 \cos^2\alpha_0}{\sin^2\alpha_0} \geq 0 \end{cases} \tag{27}$$

After the simplification, the criterion can be rewritten as

$$\begin{cases} d < 0 & (\text{if } \Omega_{\mathrm{s}} > 0) \\ d \geq \dfrac{I_t \cdot \omega_0^2 \cdot (1 + \cos\alpha_0)^2}{p_s \cdot A \cdot \sin^2\alpha_0} & (\text{if } \Omega_{\mathrm{s}} < 0) \end{cases} \tag{28}$$

The criterion indicates that the stability of the attitude equilibrium position is relevant to the spin orientation or the cm/cp offset side. The required passive station keeping can be designed by selecting proper cm/cp offset based on the stability criterion.

The stability of the equilibrium is validated via numerical simulation using the dynamics (7), (5) and (18). The case of a circular

Table 2
The relevant parameters in the design model simulation.

Parameters	Value
Sail area size (A)	3200 m^2
Mass of the solar sail (m)	200 kg
Rotational inertia (I_t/I_s)	1900/3800 kg m^2
SRP coefficients ($p_s/p_{n1}/p_{n2}$)	$3.17\times10^{-5}/1.63\times10^{-4}/1.164\times10^{-5}$ Pa
Attitude equilibrium ($\boldsymbol{\Lambda}_0$)	$\phi_0=0°$ or $180°/\alpha_0=-35.5°/\psi_0=0°$

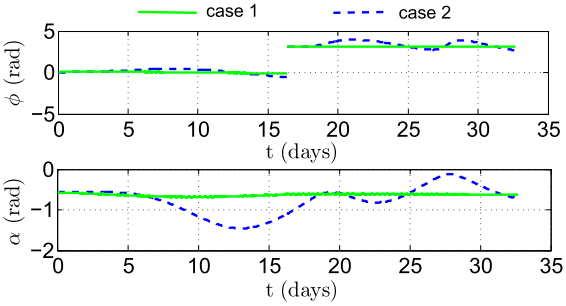

Fig. 1. Attitude response corresponding to case 1 and case 2.

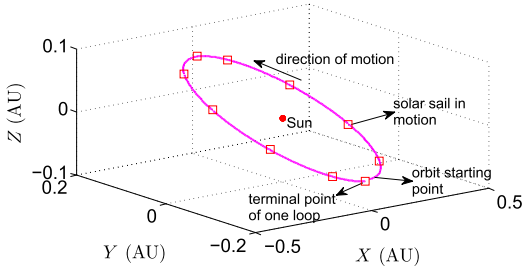

Fig. 2. The trajectory path of solar sail in the IRF over one loop.

orbit of 0.2 AU for inclination cranking is considered here. In the simulation, the variation of the orbital angular velocity and SRP coefficients is taken into account. Classic orbit elements are applied to describe the orbit of solar sail. The initial orbit value is: semi-major axis is 0.2 AU, eccentricity is zero, RAAN is zero, periapsis angle is $-90°$, true anomaly is zero. Table 2 gives the other parameters in simulation.

It is known from the criterion (28) not all equilibrium positions are stable. To validate this stability criterion, two perturbation cases around attitude equilibrium point are compared. Case 1 represents the equilibrium position is designed based on the attitude equilibrium condition (20) and stability criterion (28), whereas case 2 does not meet criterion (28). The spin angle velocity in case 1 is set to $\Omega_s=-3\times10^{-2}$ rad/s while the case 2 is set to $\Omega_s=-3\times10^{-6}$ rad/s. The corresponding cm/cp offsets are 0.45 cm and 4.5×10^{-5} cm. The same perturbation $\delta\boldsymbol{\Lambda}=[0.05\ 0.05\ 0]^{\mathrm{T}}$ is exerted on the two cases. The attitude Euler angles responses over one orbital loop corresponding to the two cases are shown in Fig. 1. It can be seen that the response of case 1 is stable around the equilibrium while the attitude angle α of case 2 is far away the equilibrium station after seven or eight days.

Fig. 2 gives the trajectory path of solar sail and Fig. 3 gives the profiles of the classical orbital elements during one loop when the initial attitude is set to $\boldsymbol{\Lambda}_0$. In the simulation, the large maneuver after half loop is assumed to be finished instantly. It can be seen that the inclination of the orbit increases continuously as expected. The distance of the sun-sail increases during half loop and then it is reduced to almost its initial value.

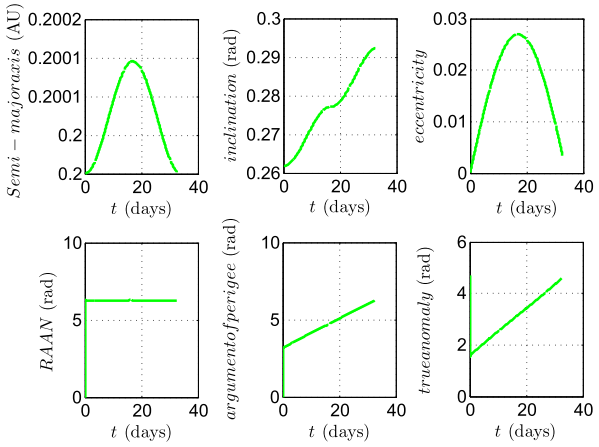

Fig. 3. The profiles of the classical orbital elements over one loop.

3. The passive station keeping of a flexible solar sail

Section 2 studies the station keeping of a rigid solar sail considering the orbit and attitude separately. However, the main characteristics of solar sail is that the sail is very flexible compared to regular spacecraft. Many differences exist between the rigid and flexible model. For example, except for the flexibility impact on structural parameter, the deformation of the solar sail will influence the unique propulsion—the SRP force. Many works have been done in studying the influence of structural vibrations [12–19]. Based on the prior studies of a finite-element (FE) model, Li et al. [20,21] developed a reduced dynamical model of a flexible sail with a hybrid coordinate method in the reference floating frame, and the satisfactory accuracy and efficiency were verified using the nonlinear FE software ABAQUS/Explicit. This high-fidelity model of a flexible solar sail is adopted in this paper to investigate the impact of sail vibration on the passive stability design of solar sail. As a further work of the high-fidelity model, the change of total SRP force on account of the sail deformation is considered in this paper and it is approximately calculated using the FE-based method. The outline of this section (section 3) is as follows. Firstly, the reduced dynamical model of a flexible solar sail is introduced. Then, some comparative studies are presented to analyze the orbit and attitude of a flexible solar sail. The comparative simulations focus on the influence of attitude–orbit coupling and the influence of oscillation–orbit–attitude coupling. In addition, two steps are divided in the study of the oscillation–orbit–attitude coupling analysis to analyze the impact of the structural parameters and the SRP force produced by sail deformation respectively. Finally, attempt to stabilize the station of a flexible solar sail is provided.

3.1. Dynamical model of flexible solar sail

3.1.1. Reduced model and formulations

The oscillation–attitude–orbit dynamical equation in vector form can be written as [20,21]

$$\begin{cases} m\ddot{\boldsymbol{R}}_{\mathrm{O}}-\boldsymbol{S}_{\mathrm{f}}\times\dot{\boldsymbol{\omega}}+\displaystyle\int_V \boldsymbol{u}_{\mathrm{f}}''\mathrm{d}m+\boldsymbol{Q}_{\mathrm{ft}}=\boldsymbol{F}_{\mathrm{t}}+\boldsymbol{F}_{\mathrm{gt}} \\ \boldsymbol{S}_{\mathrm{f}}\times\ddot{\boldsymbol{R}}_{\mathrm{O}}+\boldsymbol{J}_{\mathrm{f}}\cdot\dot{\boldsymbol{\omega}}+\displaystyle\int_V(\boldsymbol{r}_{\mathrm{f}}+\boldsymbol{u}_{\mathrm{f}})\times\boldsymbol{u}_{\mathrm{f}}''\mathrm{d}m+\boldsymbol{Q}_{\mathrm{fr}}=\boldsymbol{F}_{\mathrm{r}}+\boldsymbol{F}_{\mathrm{gr}} \\ \boldsymbol{C}_{\mathrm{t}}^{\mathrm{T}}\cdot\ddot{\boldsymbol{R}}_{\mathrm{O}}+\boldsymbol{C}_{\mathrm{r}}^{\mathrm{T}}\cdot\dot{\boldsymbol{\omega}}+\displaystyle\int_V\boldsymbol{\Phi}_{\mathrm{NL}}^{\mathrm{T}}\cdot\boldsymbol{u}_{\mathrm{f}}''\mathrm{d}m+\boldsymbol{K}_{\mathrm{f}}\boldsymbol{q}+\boldsymbol{Q}_{\mathrm{ff}}=\boldsymbol{F}_{\mathrm{f}}+\boldsymbol{F}_{\mathrm{gf}} \end{cases} \tag{29}$$

where

$$\boldsymbol{S}_{\mathrm{f}} = \int_V (\boldsymbol{r}_{\mathrm{f}} + \boldsymbol{u}_{\mathrm{f}})\mathrm{d}m \tag{30}$$

$$\boldsymbol{J}_{\mathrm{f}} = \int_V \left[(\boldsymbol{r}_{\mathrm{f}} + \boldsymbol{u}_{\mathrm{f}}) \cdot (\boldsymbol{r}_{\mathrm{f}} + \boldsymbol{u}_{\mathrm{f}})\boldsymbol{I}_3 - (\boldsymbol{r}_{\mathrm{f}} + \boldsymbol{u}_{\mathrm{f}})(\boldsymbol{r}_{\mathrm{f}} + \boldsymbol{u}_{\mathrm{f}})\right]\mathrm{d}m \tag{31}$$

$$\boldsymbol{\Phi}_{\mathrm{NL}} = \begin{pmatrix} -z\frac{\delta \boldsymbol{\Phi}}{\delta x} - \boldsymbol{q}^{\mathrm{T}} \cdot \int_{x_0}^{x} \frac{\delta \boldsymbol{\Phi}^T}{\delta x}\frac{\delta \boldsymbol{\Phi}}{\delta x}\mathrm{d}x \\ -z\frac{\delta \boldsymbol{\Phi}}{\delta y} - \boldsymbol{q}^{\mathrm{T}} \cdot \int_{y_0}^{y} \frac{\delta \boldsymbol{\Phi}^T}{\delta y}\frac{\delta \boldsymbol{\Phi}}{\delta y}\mathrm{d}y \\ \boldsymbol{\Phi} \end{pmatrix} \tag{32}$$

$$\boldsymbol{C}_{\mathrm{t}} = \int_V \boldsymbol{\Phi}_{\mathrm{NL}} dm \tag{33}$$

$$\boldsymbol{C}_{\mathrm{r}} = \int_V (\boldsymbol{r}_{\mathrm{f}} + \boldsymbol{u}_{\mathrm{f}}) \times \boldsymbol{\Phi}_{\mathrm{NL}}\mathrm{d}m \tag{34}$$

$$\boldsymbol{Q}_{\mathrm{ft}} = \boldsymbol{\omega} \times (\boldsymbol{\omega} \times \boldsymbol{S}_{\mathrm{f}}) + 2\boldsymbol{\omega} \times \int_V \boldsymbol{u}_{\mathrm{f}}'\mathrm{d}m \tag{35}$$

$$\boldsymbol{Q}_{\mathrm{fr}} = \boldsymbol{\omega} \times (\boldsymbol{J}_{\mathrm{f}} \cdot \boldsymbol{\omega}) + 2\int_V (\boldsymbol{r}_{\mathrm{f}} + \boldsymbol{u}_{\mathrm{f}}) \times \left(\boldsymbol{\omega} \times \boldsymbol{u}_{\mathrm{f}}'\right)\mathrm{d}m \tag{36}$$

$$\boldsymbol{Q}_{\mathrm{ff}} = \int_V \boldsymbol{\Phi}_{\mathrm{NL}}^{\mathrm{T}} \cdot \left[\boldsymbol{\omega} \times \boldsymbol{\omega} \times (\boldsymbol{r}_{\mathrm{f}} + \boldsymbol{u}_{\mathrm{f}})2\boldsymbol{\omega} \times \boldsymbol{u}_{\mathrm{f}}'\right]\mathrm{d}m \tag{37}$$

$$\boldsymbol{F}_{\mathrm{t}} = \int_A \boldsymbol{p}_{\mathrm{sun}}\mathrm{d}A \tag{38}$$

$$\boldsymbol{F}_{\mathrm{t}} = \int_A (\boldsymbol{r}_{\mathrm{f}} + \boldsymbol{u}_{\mathrm{f}}) \times \boldsymbol{p}_{\mathrm{sun}}\mathrm{d}A \tag{39}$$

$$\boldsymbol{F}_{\mathrm{f}} = \int_A \boldsymbol{\Phi}_{\mathrm{NL}}^{\mathrm{T}} \cdot \boldsymbol{p}_{\mathrm{sun}}\mathrm{d}A \tag{40}$$

$$\boldsymbol{F}_{\mathrm{gt}} = -\frac{m\mu}{R_{\mathrm{O}}^3}\boldsymbol{R}_{\mathrm{O}} - \frac{\mu}{R_{\mathrm{O}}^3}\boldsymbol{S}_{\mathrm{f}} + \frac{3\mu}{R_{\mathrm{O}}^5}\int_V \left((\boldsymbol{r}_{\mathrm{f}} + \boldsymbol{u}_{\mathrm{f}}) \cdot \boldsymbol{R}_{\mathrm{O}}\right)\boldsymbol{R}\mathrm{d}m \tag{41}$$

$$\boldsymbol{F}_{\mathrm{gr}} = -\frac{\mu}{R_{\mathrm{O}}^3}\boldsymbol{S}_{\mathrm{f}} \times \boldsymbol{R}_{\mathrm{O}} + \frac{3\mu}{R_{\mathrm{O}}^5}\int_V (\boldsymbol{r}_{\mathrm{f}} + \boldsymbol{u}_{\mathrm{f}}) \times \left((\boldsymbol{r}_{\mathrm{f}} + \boldsymbol{u}_{\mathrm{f}}) \cdot \boldsymbol{R}_{\mathrm{O}}\right)\boldsymbol{R}_{\mathrm{O}}\mathrm{d}m \tag{42}$$

$$\boldsymbol{F}_{\mathrm{gf}} = -\frac{\mu}{R_{\mathrm{O}}^3}\boldsymbol{C}_{\mathrm{t}}^{\mathrm{T}}\boldsymbol{R}_{\mathrm{O}} - \frac{\mu}{R_{\mathrm{O}}^3}\int_V \boldsymbol{\Phi}_{\mathrm{NL}}^{\mathrm{T}} \cdot (\boldsymbol{r}_{\mathrm{f}} + \boldsymbol{u}_{\mathrm{f}})\mathrm{d}m + \frac{3\mu}{R_{\mathrm{O}}^5}\int_V \boldsymbol{\Phi}_{\mathrm{NL}}^{\mathrm{T}}\left((\boldsymbol{r}_{\mathrm{f}} + \boldsymbol{u}_{\mathrm{f}}) \cdot \boldsymbol{R}_{\mathrm{O}}\right)\boldsymbol{R}\mathrm{d}m \tag{43}$$

The physical meaning of the above variables, the operation of $(\dot{})(\ddot{})$ $(')('')$, can refer to the NOMENCLATURE at the beginning of the paper.

3.1.2. Finite element modeling

A FE model conducted by ABAQUS is adopted to calculate the modal integral constants in Eq. (29). The model is composed of a hub, and a large square membrane, as shown in Fig. 4.

The two parts in the model are illustrated in detail as follows.

- Hub part: The shape of the hub is assumed to be a cylinder with a height of 1 m, the mass of 500 kg. Deformable solid part is used for the hub model in ABAQUS and 544 elements are divided. It is noted that the rigidity of the hub is not considered. So rigid constraint is applied to the hub, that is, the hub is considered a rigid body. The motion of the hub is transferred to the sail membrane by setting the kinematic coupling constraint in the software.
- Sail membrane part: The sail membrane is a square film with a hole in the center. The film is of 2.50 μm in thickness with metallic coatings. Density = 1572 kg/m^3; Young's Modulus = 2.48 GPa; Poisson's ratio = 0.34. The distance from the center to the tip is 40 m. The sail part is divided into 3014 S3R shell elements.

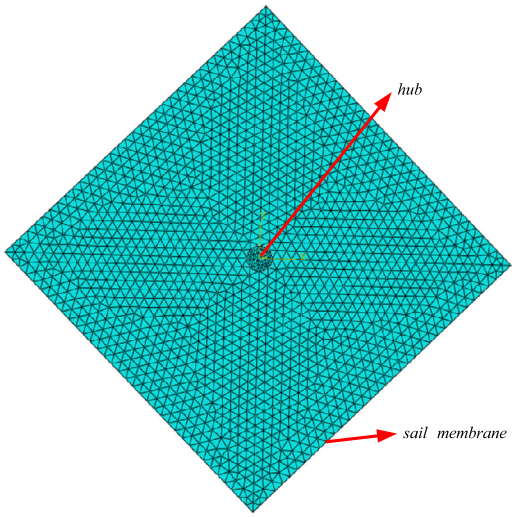

Fig. 4. FE model of the solar sail.

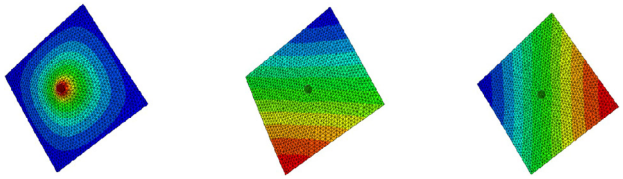

(a) Mode 1 at 0.0491842 Hz (b) Mode 2 at 0.0824752 Hz (c) Mode 3 at 0.0824810 Hz

Fig. 5. The first three non-rigid modes of the solar sail at spin angle velocity 0.1 rad per second.

Table 3
The natural frequencies corresponding to different spin rate.

Spin angular velocity	First-order frequency (Hz)	Second-order frequency (Hz)	Third-order frequency (Hz)
−0.03	0.0147564	0.02417	0.02417
−0.1	0.0491842	0.0824752	0.0824752
−0.3	0.14751	0.24737	0.24738
−0.8	0.39331	0.65980	0.65985
−1.2	0.58961	2.0114	2.1624

Centrifugal force is exerted on the membrane to get the required modes. A modal analysis step is created to generate the frequencies and mode shapes of the solar sail. As an example, when the spin angle velocity is −0.1 rad/s, the preceding three non-rigid modes at the corresponding frequency are shown in Fig. 5. In the latter simulations, different spin rates are considered and their natural frequencies and modes are different too, which are listed in Table 3. It is verified from the generated data file in ABAQUS that the effective mass of the preceding three modes contributes 95% in the total mass along the norm direction. Based on the FE theory, the foreshortened modes can reflect the dynamic characteristic effectively.

3.2. Comparative studies

3.2.1. Attitude–orbit dynamics of rigid model

Rather than the attitude and orbit dynamics separately (called design dynamical model), the attitude–orbit dynamics model is applied to study the attitude–orbit coupling impact in the passive station keeping of a rigid spinning solar. The attitude–orbit dynamics can be obtained by eliminating the items related to the vibration in Eq. (29)

$$\begin{cases} m\ddot{\boldsymbol{R}}_{\mathrm{O}} - \boldsymbol{S}_0 \times \dot{\boldsymbol{\omega}} = \boldsymbol{F}_{\mathrm{t}} + \boldsymbol{F}_{\mathrm{gt}} - \boldsymbol{\omega} \times (\boldsymbol{\omega} \times \boldsymbol{S}_0) \\ \boldsymbol{S}_0 \times \ddot{\boldsymbol{R}}_{\mathrm{O}} + \boldsymbol{J}_0 \cdot \dot{\boldsymbol{\omega}} = \boldsymbol{F}_{\mathrm{r}} + \boldsymbol{F}_{\mathrm{gr}} - \boldsymbol{\omega} \times (\boldsymbol{J}_0 \cdot \boldsymbol{\omega}) \end{cases} \tag{44}$$

Eq. (44) can be written in the BRF as follows

$$\begin{bmatrix} m \cdot \boldsymbol{I}_3 & -\tilde{\boldsymbol{S}}_0^b \\ \tilde{\boldsymbol{S}}_0^b & \boldsymbol{J}_0^b \end{bmatrix} \cdot \begin{bmatrix} \ddot{\boldsymbol{R}}_{\mathrm{O}}^{\mathrm{b}} \\ \dot{\boldsymbol{\omega}}_{\mathrm{b}} \end{bmatrix} = \begin{bmatrix} \boldsymbol{F}_{\mathrm{t}}^{\mathrm{b}} + \boldsymbol{F}_{\mathrm{gt}}^{\mathrm{b}} - \boldsymbol{\omega}_{\mathrm{b}} \times (\boldsymbol{\omega}_{\mathrm{b}} \times \boldsymbol{S}_0^{\mathrm{b}}) \\ \boldsymbol{F}_{\mathrm{r}}^{\mathrm{b}} + \boldsymbol{F}_{\mathrm{gr}}^{\mathrm{b}} - \boldsymbol{\omega}_{\mathrm{b}} \times (\boldsymbol{J}_0^{\mathrm{b}} \cdot \boldsymbol{\omega}_{\mathrm{b}}) \end{bmatrix} \tag{45}$$

where

$$\boldsymbol{S}_0^{\mathrm{b}} = m \cdot \boldsymbol{\rho}_{\mathrm{C}}^{\mathrm{b}} \tag{46}$$

$$\boldsymbol{J}_0^{\mathrm{b}} = \boldsymbol{J}_{\mathrm{c}} + m \cdot \left[d^2 \cdot \boldsymbol{I}_3 - \boldsymbol{\rho}_{\mathrm{C}}^{\mathrm{b}} \cdot \left(\boldsymbol{\rho}_{\mathrm{C}}^{\mathrm{b}} \right)^T \right] \tag{47}$$

$$\boldsymbol{F}_{\mathrm{t}}^{\mathrm{b}} = \boldsymbol{F}_b \tag{48}$$

$$\boldsymbol{F}_{\mathrm{r}}^{\mathrm{b}} = \boldsymbol{T}_o \tag{49}$$

The angular acceleration can be replaced by the twice differential of Euler angles

$$\dot{\boldsymbol{\omega}}_{\mathrm{b}} = \boldsymbol{A}_{\mathrm{brf}} \cdot \boldsymbol{A}_{\Lambda} \cdot \ddot{\boldsymbol{\Lambda}} + \boldsymbol{A}_{\mathrm{brf}} \cdot \boldsymbol{d\omega}_1 + \boldsymbol{d\omega}_2 \tag{50}$$

where

$$\ddot{\boldsymbol{\Lambda}} = \begin{bmatrix} \ddot{\phi} & \ddot{\alpha} & \ddot{\psi} \end{bmatrix}^{\mathrm{T}} \tag{51}$$

$$\boldsymbol{d\omega}_1 = \begin{bmatrix} \cos\alpha \cdot \sin\psi \cdot \dot{\alpha} + \sin\alpha \cdot \cos\psi \cdot \dot{\psi} & -\sin\psi \cdot \dot{\psi} & 0 \\ \cos\alpha \cdot \cos\psi \cdot \dot{\alpha} - \sin\alpha \cdot \sin\psi \cdot \dot{\psi} & -\cos\psi \cdot \dot{\psi} & 0 \\ -\sin\alpha \cdot \dot{\alpha} & 0 & 0 \end{bmatrix} \cdot \begin{bmatrix} \dot{\phi} \\ \dot{\alpha} \\ \dot{\psi} \end{bmatrix} \tag{52}$$

$$\boldsymbol{d\omega}_2 = \Omega_{\mathrm{s}} \cdot \begin{bmatrix} -\sin\Omega_{\mathrm{s}}t \cdot (\cos\psi \cdot \sin\phi \cdot \omega_{\mathrm{o}} + \sin\psi \cdot \cos\alpha \cdot \cos\phi \cdot \omega_{\mathrm{o}} + \omega_x) \\ +\cos\Omega_{\mathrm{s}}t \cdot (-\sin\psi \cdot \sin\phi \cdot \omega_{\mathrm{o}} + \cos\psi \cdot \cos\alpha \cdot \cos\phi \cdot \omega_{\mathrm{o}} + \omega_y) \\ -\cos\Omega_{\mathrm{s}}t \cdot (\cos\psi \cdot \sin\phi \cdot \omega_{\mathrm{o}} + \sin\psi \cdot \cos\alpha \cdot \cos\phi \cdot \omega_{\mathrm{o}} + \omega_x) \\ -\sin\Omega_{\mathrm{s}}t \cdot (-\sin\psi \cdot \sin\phi \cdot \omega_{\mathrm{o}} + \cos\psi \cdot \cos\alpha \cdot \cos\phi \cdot \omega_{\mathrm{o}} + \omega_y) \\ 0 \end{bmatrix} \tag{53}$$

Substitute Eqs. (50)–(53) into (45) and the attitude–orbit dynamics in the BRF can be rewritten as

$$\begin{bmatrix} m \cdot \boldsymbol{I}_3 & -\tilde{\boldsymbol{S}}_0^{\mathrm{b}} \cdot \boldsymbol{A}_{\mathrm{brf}} \cdot \boldsymbol{A}_{\Lambda} \\ \tilde{\boldsymbol{S}}_0^{\mathrm{b}} & \boldsymbol{J}_0^{\mathrm{b}} \cdot \boldsymbol{A}_{\mathrm{brf}} \cdot \boldsymbol{A}_{\Lambda} \end{bmatrix} \cdot \begin{bmatrix} \ddot{\boldsymbol{R}}_{\mathrm{O}}^{\mathrm{b}} \\ \ddot{\boldsymbol{\Lambda}} \end{bmatrix} = \begin{bmatrix} \boldsymbol{F}_{\mathrm{t}}^{\mathrm{b}} + \boldsymbol{F}_{\mathrm{gt}}^{\mathrm{b}} - \boldsymbol{\omega}_{\mathrm{b}} \times (\boldsymbol{\omega}_{\mathrm{b}} \times \boldsymbol{S}_0^{\mathrm{b}}) \\ \boldsymbol{F}_{\mathrm{r}}^{\mathrm{b}} + \boldsymbol{F}_{\mathrm{gr}}^{\mathrm{b}} - \boldsymbol{\omega}_{\mathrm{b}} \times (\boldsymbol{J}_0^{\mathrm{b}} \cdot \boldsymbol{\omega}_{\mathrm{b}}) \end{bmatrix} - \begin{bmatrix} -\tilde{\boldsymbol{S}}_0^{\mathrm{b}} \\ \boldsymbol{J}_0^{\mathrm{b}} \end{bmatrix} \cdot (\boldsymbol{A}_{\mathrm{brf}} \cdot \boldsymbol{d\omega}_1 \cdot \boldsymbol{d\omega}_2) \tag{54}$$

Eq. (54) can be integrated directly to get the orbit information in the IRF and the attitude response in the ORF.

3.2.2. Oscillation–attitude–orbit dynamics of a flexible model

The oscillation–attitude–orbit dynamics can be obtained by projecting the vector equations (29) into the BRF, which is

$$\begin{pmatrix} m\boldsymbol{I}_3 & -\tilde{\boldsymbol{S}}_{\mathrm{f}}^{\mathrm{b}} & \boldsymbol{C}_{\mathrm{t}}^{\mathrm{b}} \\ \tilde{\boldsymbol{S}}_{\mathrm{f}}^{\mathrm{b}} & \boldsymbol{J}_{\mathrm{f}}^{\mathrm{b}} & \boldsymbol{C}_{\mathrm{r}}^{\mathrm{b}} \\ (\boldsymbol{C}_{\mathrm{t}}^{\mathrm{b}})^{\mathrm{T}} & (\boldsymbol{C}_{\mathrm{r}}^{\mathrm{b}})^{\mathrm{T}} & \boldsymbol{M}_{\mathrm{f}} \end{pmatrix} \begin{pmatrix} \ddot{\boldsymbol{R}}_{\mathrm{O}}^{\mathrm{b}} \\ \dot{\boldsymbol{\omega}}^{\mathrm{b}} \\ \ddot{\boldsymbol{q}} \end{pmatrix} + \begin{pmatrix} \boldsymbol{0}_{3\times3} & \boldsymbol{0}_{3\times3} & \boldsymbol{0}_{3\times n} \\ \boldsymbol{0}_{3\times3} & \boldsymbol{0}_{3\times3} & \boldsymbol{0}_{3\times n} \\ \boldsymbol{0}_{n\times3} & \boldsymbol{0}_{n\times3} & \boldsymbol{K}_{\mathrm{f}} \end{pmatrix} \begin{pmatrix} \boldsymbol{R}_{\mathrm{O}}^{\mathrm{b}} \\ \boldsymbol{\Lambda} \\ \boldsymbol{q} \end{pmatrix} = \begin{pmatrix} \boldsymbol{F}_{\mathrm{t}} + \boldsymbol{F}_{\mathrm{gt}} - \boldsymbol{Q}_{\mathrm{ft}} \\ \boldsymbol{F}_{\mathrm{r}} + \boldsymbol{F}_{\mathrm{gr}} - \boldsymbol{Q}_{\mathrm{fr}} \\ \boldsymbol{F}_{\mathrm{f}} + \boldsymbol{F}_{\mathrm{gf}} - \boldsymbol{Q}_{\mathrm{ff}} \end{pmatrix} \tag{55}$$

where the normalized mass matrix is

$$\boldsymbol{M}_f = \int_V \boldsymbol{\Phi}^T \boldsymbol{\Phi} dm = \boldsymbol{I}_n \tag{56}$$

the modal stiffness matrix is

$$\boldsymbol{K}_f = \mathrm{diag}\left(\Omega_1^2, \Omega_2^2, \ldots, \Omega_n^2\right) \tag{57}$$

where Ω_i $(i = 1, 2, \ldots, n)$ is the ith-order modal angular frequency.

Substitute Eqs. (50)–(53) into (55), and the oscillation–attitude–orbit dynamical equations can be rewritten as

$$\begin{pmatrix} m_{\mathrm{tot}}\boldsymbol{I}_3 & -\tilde{\boldsymbol{S}}_{\mathrm{f}}^{\mathrm{b}} \cdot \boldsymbol{A}_{\mathrm{brf}} \cdot \boldsymbol{A}_{\Lambda} & \boldsymbol{C}_{\mathrm{t}}^{\mathrm{b}} \\ \tilde{\boldsymbol{S}}_{\mathrm{f}}^{\mathrm{b}} & \boldsymbol{J}_{\mathrm{f}}^{\mathrm{b}} \cdot \boldsymbol{A}_{\mathrm{brf}} \cdot \boldsymbol{A}_{\Lambda} & \boldsymbol{C}_{\mathrm{r}}^{\mathrm{b}} \\ (\boldsymbol{C}_{\mathrm{t}}^{\mathrm{b}})^{\mathrm{T}} & (\boldsymbol{C}_{\mathrm{r}}^{\mathrm{b}}) \cdot \boldsymbol{A}_{\mathrm{brf}} \cdot \boldsymbol{A}_{\Lambda} & \boldsymbol{M}_{\mathrm{f}} \end{pmatrix} \begin{pmatrix} \ddot{\boldsymbol{R}}_{\mathrm{O}}^{\mathrm{b}} \\ \ddot{\boldsymbol{\Lambda}} \\ \ddot{\boldsymbol{q}} \end{pmatrix} + \begin{pmatrix} \boldsymbol{0}_{3\times3} & \boldsymbol{0}_{3\times3} & \boldsymbol{0}_{3\times n} \\ \boldsymbol{0}_{3\times3} & \boldsymbol{0}_{3\times3} & \boldsymbol{0}_{3\times n} \\ \boldsymbol{0}_{n\times3} & \boldsymbol{0}_{n\times3} & \boldsymbol{K}_{\mathrm{f}} \end{pmatrix} \begin{pmatrix} \boldsymbol{R}_{\mathrm{O}}^{\mathrm{b}} \\ \boldsymbol{\Lambda} \\ \boldsymbol{q} \end{pmatrix} = \begin{pmatrix} \boldsymbol{F}_{\mathrm{t}} + \boldsymbol{F}_{\mathrm{gt}} - \boldsymbol{Q}_{\mathrm{ft}} \\ \boldsymbol{F}_{\mathrm{r}} + \boldsymbol{F}_{\mathrm{gr}} - \boldsymbol{Q}_{\mathrm{fr}} \\ \boldsymbol{F}_{\mathrm{f}} + \boldsymbol{F}_{\mathrm{gf}} - \boldsymbol{Q}_{\mathrm{ff}} \end{pmatrix} - \begin{pmatrix} -\tilde{\boldsymbol{S}}_{\mathrm{f}}^{\mathrm{b}} \\ \boldsymbol{J}_{\mathrm{f}}^{\mathrm{b}} \\ (\boldsymbol{C}_{\mathrm{r}}^{\mathrm{b}})^{\mathrm{T}} \end{pmatrix} \cdot (\boldsymbol{A}_{\mathrm{brf}} \cdot \boldsymbol{d\omega}_1 + \boldsymbol{d\omega}_2) \tag{58}$$

The orbit profile, attitude response with respect to the ORF and the vibration can be obtained by integrating Eq. (58) directly. It should be noted that two models are provided for the SRP force in Eq. (58) in the paper, as shown in Eqs. (59) and (67).

3.2.3. Total SRP force experienced by the deformed sail

In most prior studies of flexible solar sail with a plane membrane, the deformation is usually ignored to calculate the SRP force [17–21]. There are two main reasons for the simplified process. One is that the deformation is much smaller compared to the area size and the sail is approximately still a plane. The other reason is that the real-time shape of the sail is usually difficult to describe in an analytical way. However, the vibration of the sail membrane will make the sail non-planar and influence the SRP force inevitably. To investigate the impact of the SRP due to the oscillation, two SRP models are presented respectively. One is based on the plane assumption same as the prior work, which is called SRP model-1. The other SRP model is calculated based on the FE method, which is called SRP model-2 in this paper. The SRP of model-1 is related to the sail attitude and distance from sun, whereas SRP of model-2 is related to the sail oscillation apart from the attitude and distance.

The same as the rigid model, the SRP model-1 is represented as

$$\boldsymbol{F}_{\mathrm{t}}^{(1)} = \boldsymbol{F}_{\mathrm{b}}$$

$$\boldsymbol{F}_{\mathrm{r}}^{(1)} = \boldsymbol{T}_{\mathrm{o}}$$

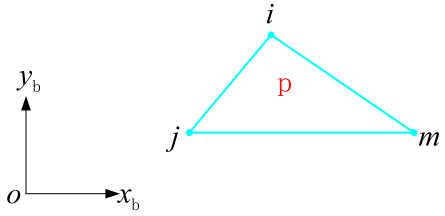

Fig. 6. A small surface of the sail membrane.

$$\boldsymbol{F}_{\mathrm{f}}^{(1)} = \int_V \boldsymbol{\Phi}_{\mathrm{NL}}^{\mathrm{T}} \mathrm{d}\boldsymbol{F}_{\mathrm{t}} = \frac{-\boldsymbol{F}_{\mathrm{t}}^{(1)}(1)\cdot\boldsymbol{C}_x^{\mathrm{T}}\cdot\boldsymbol{q} - \boldsymbol{F}_{\mathrm{t}}^{(1)}(2)\cdot\boldsymbol{C}_y^{\mathrm{T}}\cdot\boldsymbol{q}}{A\rho h} + \frac{(\int_V \boldsymbol{\Phi}\mathrm{d}m)^T\cdot\boldsymbol{F}_{\mathrm{t}}^{(1)}(3)}{\rho h} \tag{59}$$

where the $\boldsymbol{F}_{\mathrm{t}}^{(1)}(1)$, $\boldsymbol{F}_{\mathrm{t}}^{(1)}(2)$ and $\boldsymbol{F}_{\mathrm{t}}^{(1)}(3)$ are respectively the first, second and third element of $\boldsymbol{F}_{\mathrm{t}}^{(1)}$.

The SRP model-2 is developed approximately by summing the SRP force exerted on every small plane surface of the sail. The small surface is exactly the S3R shell element of the sail membrane, which is shown in Fig. 6. In the small surface, 'i, j, m' are the three node numbers of the S3R element 'p'. From the FE model, the totality of the shell nodes and elements are respectively n_tot = 1581 and e_tot = 3014.

Considering the tensile deformation is ignored, the area of the shell element can be described in the BRF as

$$A^{(p)} = \frac{1}{2}\left[(y_j - y_m)\cdot(-x_m + x_i) - (y_m - y_i)\cdot(-x_j + x_m)\right] \tag{60}$$

where x_i, y_i are the x and y coordinates of node i in the BRF.

The unit normal vector of the small surface can be represented approximately in the BRF as

$$\boldsymbol{n}_{\mathrm{b}}^{(p)} = \frac{\boldsymbol{r}_{ij}\times\boldsymbol{r}_{im}}{|\boldsymbol{r}_{ij}\times\boldsymbol{r}_{im}|} \tag{61}$$

where

$$\boldsymbol{r}_{ij} = \boldsymbol{r}_j - \boldsymbol{r}_i = \begin{bmatrix} x(j) - x(i) \\ y(j) - y(i) \\ u(j) - u(i) \end{bmatrix} \tag{62}$$

where $u(\cdot)$ is the real-time transversal displacement of the shell node, and the $\boldsymbol{r}_{im}$ is obtained in a similar way.

The total SRP propulsion calculated by summation is written as

$$\boldsymbol{F}_{\mathrm{t}}^{(2)} = \sum_{p=1}^{\mathrm{e\_tot}} A^{(p)}\cdot\boldsymbol{P}_b^{(p)} \tag{63}$$

where $\boldsymbol{P}_b^{(p)}$ is the solar radiation pressure exerted on the small surface, and it can be written as

$$\boldsymbol{P}_b^{(p)} = \left[p_s\cdot\left(\boldsymbol{s}_b\cdot\boldsymbol{n}_b^{(p)}\right)\cdot\boldsymbol{s}_b + p_{n1}\cdot\left(\boldsymbol{s}_b\cdot\boldsymbol{n}_b^{(p)}\right)^2\cdot\boldsymbol{n}_b^{(p)} + p_{n2}\cdot\left(\boldsymbol{s}_b\cdot\boldsymbol{n}_b^{(p)}\right)\cdot\boldsymbol{n}_b^{(p)}\right] \tag{64}$$

The total SRP torque calculated based on the FE method is written as

$$\boldsymbol{F}_{\mathrm{r}}^{(2)} = \sum_{p=1}^{\mathrm{e\_tot}} A^{(p)}\cdot\left(\boldsymbol{r}_{\mathrm{p}}\times\boldsymbol{P}_b^{(p)}\right) \tag{65}$$

where $\boldsymbol{r}_{\mathrm{p}}$ is the arithmetic mean value of the node coordinate matrix in the 'p' element.

The total SRP restoring force in this method can be represented as

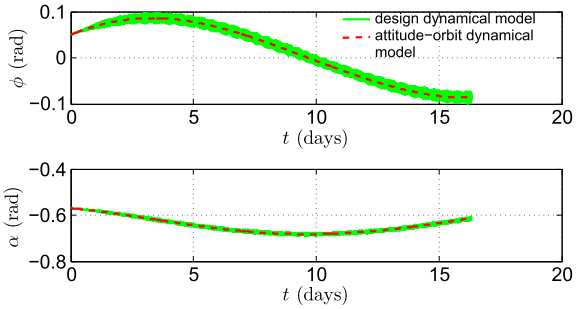

Fig. 7. The attitude response using the two models with an initial perturbation.

$$\boldsymbol{F}_{\mathrm{f}}^{(2)} = \frac{-\boldsymbol{F}_{\mathrm{t}}^{(1)}(1)\cdot\boldsymbol{C}_x^{\mathrm{T}}\cdot\boldsymbol{q} - \boldsymbol{F}_{\mathrm{t}}^{(1)}(2)\cdot\boldsymbol{C}_y^{\mathrm{T}}\cdot\boldsymbol{q}}{A\rho h} + \sum_{p=1}^{\mathrm{e\_tot}} A^{(p)}\cdot\boldsymbol{P}_b^{(p)}(3)\cdot\boldsymbol{\Phi}^{\mathrm{T}(p)} \tag{66}$$

where $\boldsymbol{P}_b^{(p)}(3)$ is the third element of $\boldsymbol{P}_b^{(p)}$ as shown in Eq. (64), $\boldsymbol{\Phi}^{\mathrm{T}(p)}$ are the arithmetic mean value of the modes of the three nodes in 'p' element.

In summary, the SRP model-2 can be written as

$$\begin{aligned} \boldsymbol{F}_{\mathrm{t}}^{(2)} &= \sum_{p=1}^{\mathrm{e\_tot}} A^{(p)}\cdot\boldsymbol{P}_b^{(p)} \\ \boldsymbol{F}_{\mathrm{r}}^{(2)} &= \sum_{p=1}^{\mathrm{e\_tot}} A^{(p)}\cdot\left(\boldsymbol{r}_p\times\boldsymbol{P}_b^{(p)}\right) \\ \boldsymbol{F}_{\mathrm{f}}^{(2)} &= \frac{-\boldsymbol{F}_{\mathrm{t}}^{(1)}(1)\cdot\boldsymbol{C}_x^{\mathrm{T}}\cdot\boldsymbol{q} - \boldsymbol{F}_{\mathrm{t}}^{(1)}(2)\cdot\boldsymbol{C}_y^{\mathrm{T}}\cdot\boldsymbol{q}}{A\rho h} + \sum_{p=1}^{\mathrm{e\_tot}} A^{(p)}\cdot\boldsymbol{P}_b^{(p)}(3)\cdot\boldsymbol{\Phi}^{\mathrm{T}(p)} \end{aligned} \tag{67}$$

3.2.4. Comparison between the attitude–orbit model and the design model

The simulation results using the attitude–orbit model and the former design model are presented to analyze the coupling impact in inclination cranking. The initial value of the orbit and the required attitude equilibrium are identical to the design model simulation case. The initial attitude perturbation $\delta\boldsymbol{\Lambda} = [0.05\ 0.05\ 0]^{\mathrm{T}}$ is exerted on the simulation to test the passive station keeping. The spin angle velocity is set to -0.03 rad/s, and the corresponding cm/cp offset is 0.9 cm. The other parameters are shown in Table 4.

On the one half loops, the attitude response and the orbit profile simulated by the two models respectively are shown in Fig. 7 and Fig. 8. It can be seen that similar stable attitude and orbit results are obtain by the design model and attitude–orbit coupling model. The similarity indicates that the attitude–orbit coupling influence is tiny in the inclination cranking. In other words, the simple dynamical model, rather than the coupling model, is applied to design the passive stability of solar sail is reasonable. With further simulation, it can be found that many small quantities exist in the attitude–orbit coupling Eq. (54). The coupling equation can be simplified by abandoning these smaller items, which becomes

$$\begin{aligned} \ddot{\boldsymbol{R}}_{\mathrm{O}}^{\mathrm{b}} &\approx \frac{\boldsymbol{F}_{\mathrm{t}}^{\mathrm{b}}}{m} - \frac{\mu}{R_{\mathrm{O}}^3}\boldsymbol{R}_{\mathrm{O}} \\ \tilde{\boldsymbol{S}}_0^b\cdot\ddot{\boldsymbol{R}}_{\mathrm{O}}^{\mathrm{b}} + \boldsymbol{J}_0^b\cdot\dot{\boldsymbol{\omega}}_{\mathrm{b}} + \boldsymbol{\omega}_{\mathrm{b}}\times\left(\boldsymbol{J}_0^{\mathrm{b}}\cdot\boldsymbol{\omega}_{\mathrm{b}}\right) &\approx \boldsymbol{T}_{\mathrm{o}} - \frac{\mu}{R_{\mathrm{O}}^3}\boldsymbol{S}_{\mathrm{O}}\times\boldsymbol{R}_{\mathrm{O}} \end{aligned} \tag{68}$$

Table 4
Parameters in the attitude–orbit model simulation.

Parameters	Values
Membrane area—A	3200 m^2
Total mass—m	515.18 kg
Rotational inertial—I_t/I_s	7720.19/3902.00 kg m^2
SRP coefficients with 0.2 AU from the sun—$p_s/p_{n1}/p_{n2}$	$3.17 \times 10^{-5}/1.63 \times 10^{-4}/1.164 \times 10^{-5}$ Pa

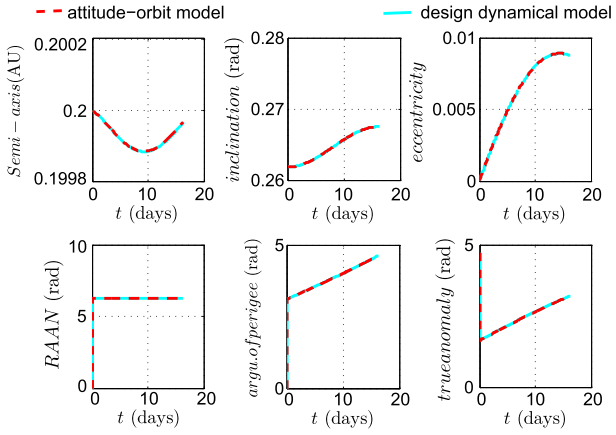

Fig. 8. The orbit elements profile using the two models.

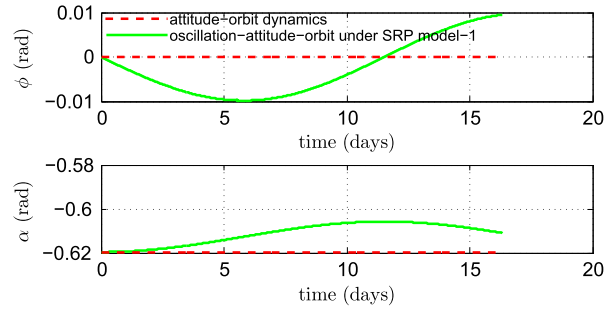

Fig. 9. The attitude responses of two models.

It can be seen that the simplified attitude–orbit coupling equation (68) are almost identical to the design dynamical model except for the little difference of rotational inertia. Thus, the simulated results by the two models are almost identical.

3.2.5. Comparison between attitude–orbit model and oscillation–attitude–orbit model under the SRP model-1

In this section, the plane assumption (refer to Eq. (59)) is applied in the flexible solar sail model to investigate the oscillation impact. The impact of the SRP difference caused by deformation will be studied in section 3.2.6. The attitude–orbit model (54) and the oscillation–attitude–orbit model (58) are used for simulation. The spin angle velocity is set to −0.3 rad/s, and the corresponding cm/cp offset is 9 cm. The initial value of the orbit and the required attitude equilibrium are identical to the design model simulation case. The initial value of the attitude is the equilibrium. The attitude responses of the attitude–orbit model and oscillation–attitude–orbit model over half loops are shown in Fig. 9. The simulation indicates that the vibration has an effect on the solar sail attitude, even with the SRP model-1. This is mainly because the static and inertia moments of a flexible solar sail is slightly different from the rigid one, while the static moment is closely related to the designed equilibrium point. When the spin rate is 0.3 rad/s, the deviation amplitude of the Euler angles from the equilibrium position is 0.01 rad during the inclination cranking without large maneuver, which is supposed to be acceptable in the engineering.

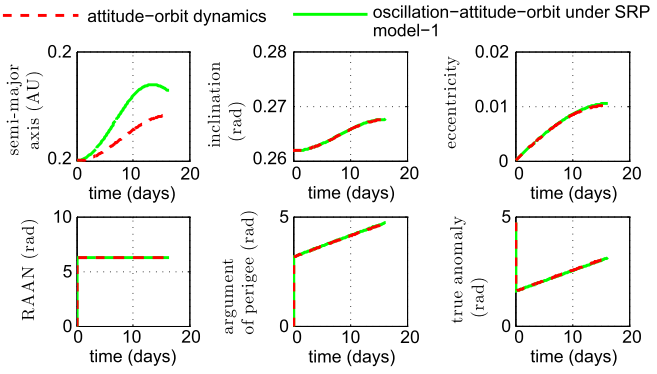

Fig. 10. The orbit elements profile of the two models.

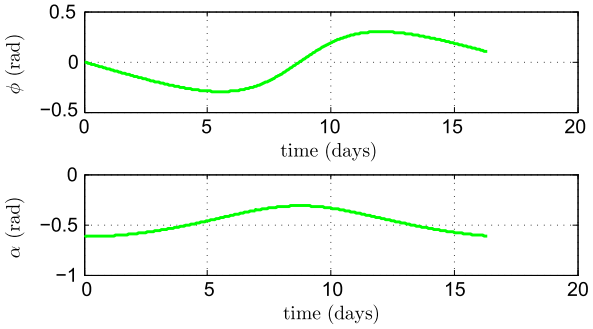

Fig. 11. The attitude response of oscillation–attitude–orbit dynamics under srp model-1 with the spin angular v0.1 rad per second.

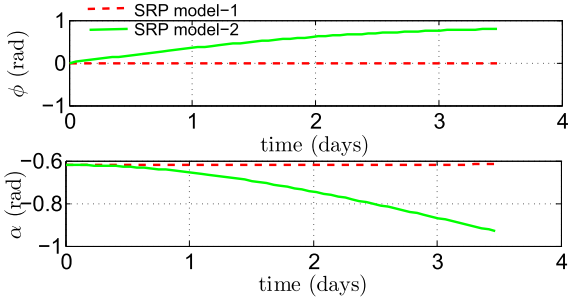

Fig. 12. The attitude response of SRP model-1 and model-2.

The orbit elements profile of the two models with this spin rate is shown in Fig. 10, which shows that the difference of the two models is tiny. After further simulation, it can be found that the impact of the oscillation on the attitude increases as the spin rate is reduced, and the impact decreases when the spin rate rises. The reason is that the lower spin rate means a larger flexibility for the no support spinning solar sail and a weaker ability to keep the orientation. For example, when the spin rate is reduced to 0.1 rad/s the attitude deviation amplitude is quite large, as is shown in Fig. 11.

3.2.6. Comparison between SRP model-1 and model-2

Section 3.2.5 verifies that the sail oscillation has an effect on the attitude and orbit even ignoring the difference of SRP force

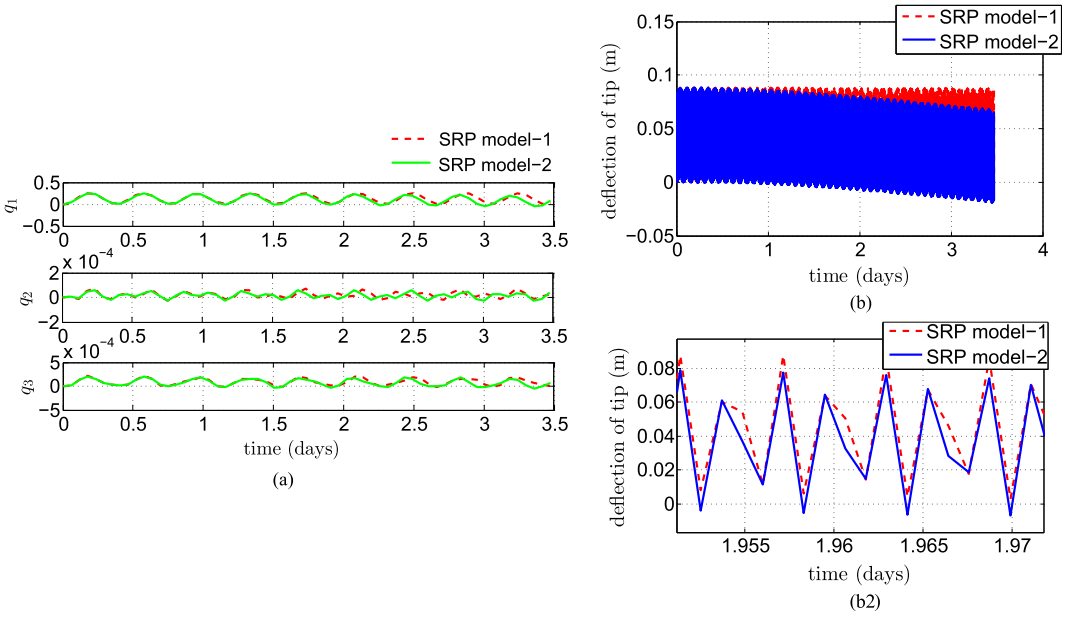

Fig. 13. (a) The responses of modal coordinate. (b) The responses of tip deflection. (b2) The partial enlarged drawing of (b).

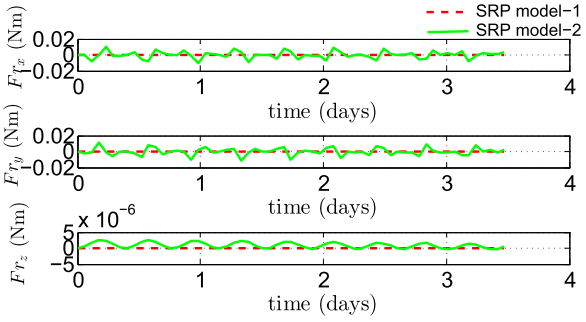

Fig. 14. The variation of the SRP torque.

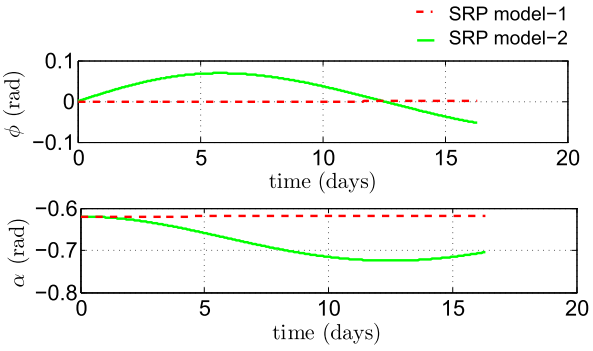

Fig. 15. The attitude response with a spin rate 0.8 rad per second.

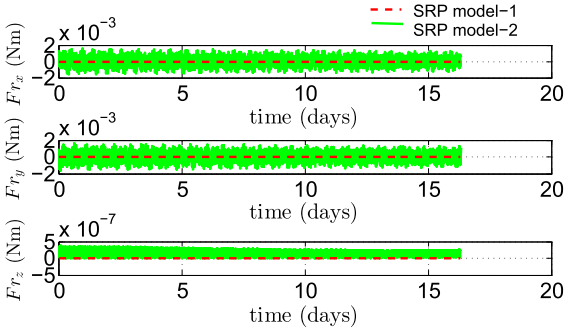

Fig. 16. The SRP torque produced by sail deformation with a spin rate 0.8 rad per second.

caused by the deformation. In this part, the same oscillation–attitude–orbit equation (58) but the different SRP models (refer to Eq. (59) and Eq. (67)) are used for simulation to analyze the SRP impact of the sail deformation. The simulation parameters are identical to section 3.2.5. When the spin angular velocity is still set to −0.3 rad/s, the attitude response of the SRP model-1 and model-2 are presented as Fig. 12. It can be seen that the prior passive station keeping under SRP model-1 is broken when the SRP impact of deformation is taken into account. The primary reason for this instability is that the SRP torque is produced by vibration, which is different to the case of SRP model-1. The vibration response of the sail and the corresponding SRP torque are shown in Fig. 13 (a, b, b2) and Fig. 14 respectively. It can be seen that the sail vibration of the two SRP models are similar, where their deflection amplitudes of sail tip is about 8 cm. The SRP torque amplitude produced by deformation is about 0.01 N m, which makes the attitude instable.

The simulation results indicate that the designed attitude equilibrium using a plane sail is not completely fit to the deformed case, especially the deflection increases. As is well known, a large spin rate will make the normal orientation of a spacecraft more stable. So one feasible option to stable the flexible solar sail is to increase the spin rate, which means larger cm/cp offset. The attitude response of the flexible solar sail with a spin angular velocity −0.8 rad/s is shown in Fig. 15. The corresponding cm/cp offset is 24 cm. It can be seen that with this large spin rate the impact of the sail oscillation is reduced compared with the prior lower spin rate. By this time, the attitude deviation amplitude from the equilibrium is 0.08 rad, while the amplitude of the SRP torque conducted by sail deformation is 0.001 N m as is presented in Fig. 16. Further simulations indicate that the larger spin rate will make the impact of sail oscillation on the attitude smaller as expected. Here gives an example of the spin rate 1.2 rad/s, corresponding to the cm/cp offset 35 cm. The attitude and SRP torque responses are shown in Fig. 17 and Fig. 18 respectively. It can be seen that the amplitudes of attitude deviation and SRP torque are smaller than the case with the spin rate 0.8 rad/s.

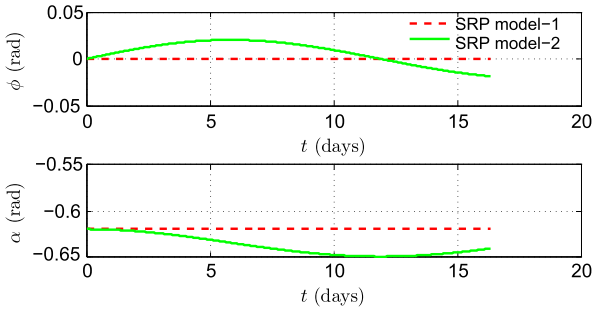

Fig. 17. The attitude response with a spin rate 1.2 rad per second.

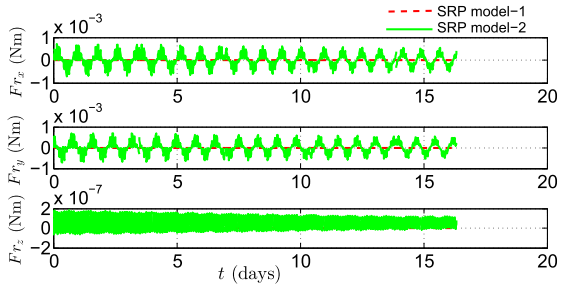

Fig. 18. The SRP torque produced by sail deformation with a spin rate 1.2 rad per second.

4. Conclusion

In this paper, the general passive stability design criterion of a flexible solar sail is investigated. As a design model, the passive station keeping during the inclination cranking of a spinning solar sail is developed using a rigid model. The design criterion shows that the required stable attitude of solar sail can be obtained passively by adjusting the cm/cp offset and the spin rate. A modal reduced oscillation–attitude–orbit model for spinning solar sail is developed to analyze the impacts of sail oscillation and the attitude–orbit coupling. The total time-varying SRP force experienced by the deformed sail is considered using the FE based method. The study indicates that the attitude–orbit coupling effect referred in this paper during the inclination cranking is tiny, whereas the oscillation has an obvious impact on the attitude and orbit of the solar sail under a certain spin rate. In the case of considering the oscillation, the original passive stability criterion by the rigid model may become invalid. The reasons of the oscillation influence are investigated via comparative simulations. The results indicate that the SRP torque due to the sail deformation and the variation of structural parameter of a flexible solar sail are the two main causes to influence the attitude and orbit. Attempt to stabilize the flexible solar sail is proposed, which is increasing the spin rate and the cm/cp offset.

Conflict of interest statement

No conflict of interest.

Acknowledgements

The authors would like to acknowledge the support from the National Natural Science Foundation of China (Grants No. 11272004) and China's civil space funding.

Appendix A. Supplementary material

Supplementary material related to this article can be found online at http://dx.doi.org/10.1016/j.ast.2016.08.005.

References

[1] J.L. West, The geostorm warning mission: enhanced opportunities based on new technology, Adv. Astronaut. Sci. 119 (102) (2004) 29–42.
[2] M. Macdonald, G.W. Hughes, et al., GeoSail: an elegant solar sail demonstration mission, J. Spacecr. Rockets 44 (4) (2007) 784–796, http://dx.doi.org/10.2514/1.22867.
[3] J.P. Sanchez, C.R. McInnes, On the ballistic capture of asteroids for resource utilization, in: 62nd International Astronautical Congress, vol. 6, 2011, pp. 4907–4921.
[4] B.E. Goldstein, A. Buffington, A.C. Cummings, et al., A solar polar sail mission: report of a study to put a scientific spacecraft in a circular polar orbit about the sun, in: Proceedings of the International Society for Optical Engineering, vol. 3442, 1998, pp. 65–76.
[5] G. Mengali, A.A. Quarta, Solar sail near-optimal circular transfers with plane change, J. Guid. Control 32 (2) (2009) 456–463, http://dx.doi.org/10.2514/1.38079.
[6] C.R. McInnes, Solar Sailing Technology, Dynamics and Mission Applications, Springer-Verlag, Berlin, 1999.
[7] C.R. McInnes, Passive control of displaced solar sail orbits, J. Guid. Control Dyn. 21 (6) (1998) 975–982, http://dx.doi.org/10.2514/2.4334.
[8] S.P. Gong, J.F. Li, H.X. Baoyin, Passive stability design for solar sail on displaced orbits, J. Spacecr. Rockets 44 (5) (2007) 1071–1080, http://dx.doi.org/10.2514/1.29752.
[9] S.P. Gong, J.F. Li, H.X. Baoyin, Analysis of displaced solar sail orbits with passive control, J. Guid. Control Dyn. 31 (3) (2008) 782–785, http://dx.doi.org/10.2514/1.32360.
[10] Y. Mimasu, T. Yamaguchi, M. Matsumoto, et al., Spinning solar sail orbit steering via spin rate control, Adv. Space Res. 48 (11) (2011) 1810–1821, http://dx.doi.org/10.1016/j.asr.2011.08.030.
[11] S.P. Gong, J.F. Li, Spin-stabilized solar sail for displaced solar orbits, Aerosp. Sci. Technol. 31 (1) (2014) 188–199, http://dx.doi.org/10.1016/j.ast.2013.10.002.
[12] S.W. Smith, H. Song, J.R. Baker, et al., Flexible models for solar sail control, in: 46th AIAA/ASME/ASCE/AHS/ASC Structures, Structural Dynamics & Materials Conference, vol. 1, 2005, pp. 11–40.
[13] T. Nakano, O. Mori, J. Kawaguchi, Stability of spinning solar sail-craft containing a huge membrane, in: International Astronautical Federation—56th International Astronautical Congress, vol. 5, 2005, pp. 2795–2804.
[14] D.W. Sleight, T. Mann, et al., Structural analysis and test comparison of a 20-meter inflation-deployed solar sail, in: 47th AIAA/ASME/ASCE/AHS/ASC Structures, Structural Dynamics, and Materials Conference, vol. 2, 2006, pp. 1408–1423.
[15] H. Sakamoto, Y. Miyazaki, K.C. Park, Finite element modeling of sail deformation under solar radiation pressure, J. Spacecr. Rockets 44 (3) (2007) 514–521, http://dx.doi.org/10.2514/1.23474.
[16] Z.Y. Sheng, J.J. Zheng, H.J. Zhou, et al., Finite element analysis about solar sail, in: IEEE International Conference on Information and Automation, 2008, pp. 1691–1696.
[17] P.W. Likins, Modal method for analysis of free rotations of spacecraft, AIAA J. 5 (7) (1967) 1304–1308, http://dx.doi.org/10.2514/3.4188.
[18] P.W. Likins, P.H. Wirsching, Use of synthetic modes in hybrid coordinate dynamic analysis, AIAA J. 6 (10) (1968) 1867–1872, http://dx.doi.org/10.2514/3.4894.
[19] B. Taleghani, D. Sleight, D. Muheim, K. Belvin, J. Wang, Assessment of analysis approaches for solar sail structural response, in: 39th AIAA/ASME/SAE/ASEE Joint Propulsion Conference and Exhibit (AIAA-2003-4796), 2003.
[20] Q. Li, T.S. Wang, X.R. Ma, Reduced model of flexible sail–boom interaction for solar sail dynamics, in: The 60th International Astronautical Congress, vol. 6, 2009, pp. 5045–5055.
[21] R.W. Zhang, Orbital and Attitude Dynamics and Control of Satellite, Beihang University, Beijing, 1998.
[22] Y. Tsuda, T. Saiki, R. Funase, et al., Generalized attitude model for spinning solar sail spacecraft, J. Guid. Control Dyn. 36 (4) (2013) 967–974, http://dx.doi.org/10.2514/1.59516.
[23] J.S. Mu, S.P. Gong, J.F. Li, Coupled control of reflectivity modulated solar sail for GeoSail formation flying, J. Guid. Control Dyn. 38 (4) (2014) 740–751, http://dx.doi.org/10.2514/1.G000117.
[24] S.P. Gong, J.F. Li, H.X. BaoYin, Formation flying solar-sail gravity tractors in displaced orbit for towing near-Earth asteroids, J. Celest. Mech. Dyn. Astron. 105 (1–3) (2009) 159–177, http://dx.doi.org/10.1007/s10569-009-9211-8.